Letter

Enhanced multichannel dual-comb spectroscopy of complex systems

Razmik Aramyan,* Oleg Tretiak, and Sushree S. Sahoo
Johannes Gutenberg-Universität Mainz, 55128 Mainz, Germany and
Helmholtz-Institut Mainz, GSI Helmholtzzentrum für Schwerionenforschung, 55128 Mainz, Germany

Dmitry Budker
Johannes Gutenberg-Universität Mainz, 55128 Mainz, Germany
Helmholtz-Institut Mainz, GSI Helmholtzzentrum für Schwerionenforschung, 55128 Mainz, Germany and
Department of Physics, University of California, Berkeley, California 94720, USA

(Received 13 March 2025; accepted 16 July 2025; published 22 August 2025)

A multichannel dual-comb spectroscopy (DCS) approach for high-resolution, broadband spectral measurements is presented, demonstrating its effectiveness in studying complex atomic systems. By implementing a photodetector array, we enhance DCS capabilities, addressing the fundamental trade-off between signal-to-noise ratio and spectral coverage. To resolve ambiguities in frequency conversion, we introduced a relative offset in beat-note frequency, ensuring accurate spectral reconstruction. As a proof of concept, the absorption spectrum of samarium (Sm) vapor is investigated over a 52-nm range, and several previously unreported absorption lines are detected. This is a step toward "Spectroscopy 2.0," enabling massively parallel spectroscopic measurements (including those at >100 T magnetic fields) crucial for atomic physics and fundamental interactions research.

DOI: 10.1103/7ktx-4h8m

Introduction. A diverse selection of atomic systems with a range of properties is essential for optimizing sensitivity to specific interactions of interest in fundamental physics experiments. This need is particularly pressing in the rapidly expanding field of search for physics beyond the Standard Model using atoms and molecules [1]. While atomic databases provide valuable spectral information [2], their coverage remains incomplete, especially for rare-earth and actinide elements. The primary reason for these gaps in atomic tables is the complexity of dense atomic spectra, which present significant challenges for both experimental measurements and theoretical modeling. In Ref. [3], an approach to spectroscopy (called Spectroscopy 2.0) is introduced, integrating three key elements: (1) a massively parallel spectroscopic tool, (2) tunable high magnetic fields that introduce additional spectroscopic dimension, and (3) advanced many-body theory enhanced by modern computational power and machine learning.

In this paper, we take the first step toward implementing Spectroscopy 2.0: development of a massively parallel spectroscopic tool. As the core technique, we employ dual-comb spectroscopy (DCS), a revolutionary method renowned for its high-resolution, high-sensitivity, and broadband spectral measurements at remarkable speed [4–7].

The two optical frequency combs used for DCS typically have repetition rates on the order of hundreds of megahertz, differing from each other by hundreds of hertz. The beat signal between the two combs is in itself a frequency comb but now in the rf domain. Each line of this comb contains information about its "parent" pair of optical frequencies. Detecting beat signals on a photodetector allows one to obtain information about the optical domain, enabling direct measurement of complex spectra, for example, complex molecular spectra in the near-infrared (NIR) range [8,9].

While DCS enables high-speed measurements within a broad wavelength range, its efficiency is constrained by the fundamental trade-off of the signal-to-noise ratio (SNR) due to several factors, including shot noise, relative intensity noise (RIN) of the laser and detector noise. In the case of a dominant light noise limit, the SNR scales as

$$\mathrm{SNR} \propto \frac{\sqrt{\tau}}{M}, \tag{1}$$

where τ is the acquisition time, and M is the number of the detected teeth of the comb [7,10]. This implies that increasing spectral coverage or reducing measurement time inherently compromises the SNR, limiting the ability to effectively study weak transitions or atoms in dynamic

*Contact author: aramyanr@uni-mainz.de

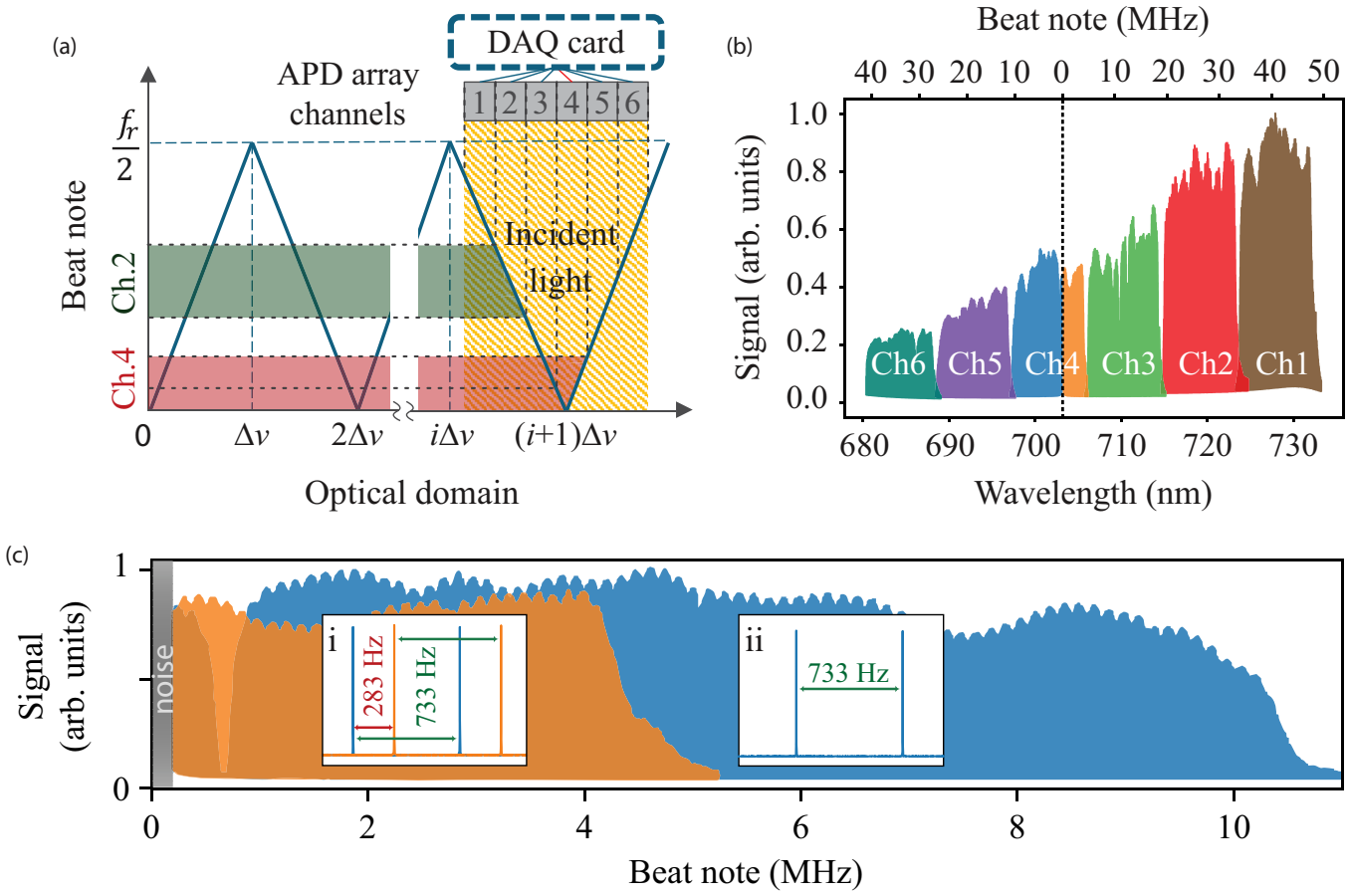

FIG. 1. Mapping of the incident light frequencies to the rf frequencies. (a) The general mapping method, with an example of ambiguous and unambiguous data. Channel 2 (unambiguous data) and channel 4 (ambiguous data) are labeled as Ch. 2 and Ch. 4, respectively. (b) The real data from six channels illustrates the signal along with its recorded rf frequencies and corresponding wavelengths. This data represents Sm spectrum at 1040 °C. (c) The normalized recorded spectrum on channel 4, where ambiguity is expected (for $\delta f_r \approx 733$ Hz). The blue and orange data represent spectra from different unambiguous regions. These components were separated during the data-analysis process. As illustrated in the two smaller enlarged figures when the two spectra overlap (i), we observe two sets of teeth with a relative offset of 283 Hz, whereas in the case of no ambiguity, we see only one set of teeth with a 733-Hz spacing (ii). Moreover in the overlapping region, a dip in the blue spectra corresponds to a strong absorption line of samarium.

systems where short acquisition time is required. Another limitation of DCS is the maximum optical range that can be acquired without aliasing when the repetition rates are fixed. The maximum optical range that can be acquired without aliasing when the repetition rates are fixed is

$$\Delta\nu = \frac{f_r^2}{2\delta f_r}, \tag{2}$$

where f_r denotes the repetition rate of one of the frequency combs and δf_r is the difference in repetition rates between the two combs [7,11]. When the recorded optical range exceeds $\Delta\nu$, the beat notes of the optical frequencies begin to alias each other, leading to ambiguity in the interpretation of the data.

We demonstrate high-SNR, ambiguity-free broadband spectroscopy of samarium (Sm, atomic number $Z = 62$). To achieve high SNR, we implement the approach proposed in Ref. [10], which suggests that in scenarios where noise is dominated by RIN, a significant gain in SNR can be achieved through the use of multiple detectors. This approach introduces additional degree of freedom in Eq. (1), adding a linear dependence on the number of detectors (assuming constant power distribution over the spectrum), as spectrally dispersing light onto multiple detectors spectrally reduces the RIN contribution per detector. These detectors must be capable of providing data separately and simultaneously in order to preserve one of the main advantages of DCS: its massively parallel nature. By selecting the repetition rates of the combs such that $k(f_{r1,2}/2)/\delta f_r$ is not an integer, where $k = 1, 2, 3, \ldots$, we introduce a relative offset between overlapping rf comb teeth, effectively resolving the ambiguity problem.

This strategy allows continued performance improvement with additional detectors, up to the point where the

dominant noise source becomes the intrinsic noise floor of the detectors themselves. This sets a practical upper limit, along with the spectral bandwidth of the laser emission. Our results demonstrate that we successfully overcome key challenges in broadband spectroscopy, probing samarium over a broad spectral range ($\Delta\lambda \approx 52$ nm) with high SNR. This enables the detection of several previously unknown transitions.

Ambiguity in frequency conversion. The beat signal between the two combs, acquired by a photodetector, contains radio frequencies, and to retrieve the corresponding optical frequencies, we must convert this rf spectrum back into optical domain. A visual representation of this frequency mapping, Fig. 1(a), can help to understand the conversion process. To ensure that only the beat note between neighboring optical lines is acquired, the maximum frequency in the rf domain (the vertical axis) should be limited to $\leq f_r/2$. The values $i\Delta\nu$, [where $i = 0, 1, 2, \ldots$ and $\Delta\nu$ is defined in Eq. (2)] delimit ith unambiguity region on the horizontal axis. The black vertical dashed lines denote the optical frequency ranges captured by each photodiode, whereas the horizontal dashed lines represent the rf frequencies of the corresponding recorded signals. To convert the rf spectrum we should start with the general representation of the optical frequencies of the comb:

$$\begin{aligned} \nu_{1n} &= f_{\mathrm{CEO1}} + nf_{r1}, \\ \nu_{2m} &= f_{\mathrm{CEO2}} + mf_{r2}, \end{aligned} \tag{3}$$

where n and m represent the tooth numbers of corresponding optical frequencies ν_{1n} and ν_{2m} of the first and second comb, respectively, and $f_{\mathrm{CEO1,2}}$ is the carrier-envelope offset. In our case, we lock the system such that $f_{\mathrm{CEO1}} = f_{\mathrm{CEO2}}$.

Since both combs contribute equally to each beat note, it is necessary to select one of them to serve as a reference for our calculation frame. We will choose the comb with the smaller repetition rate (this is an arbitrary choice); let us consider $f_{r1} < f_{r2}$. The beat note (f_{rf}) between pair of teeth is

$$f_{\mathrm{rf}} = |\nu_{1n} - \nu_{2m}| = |nf_{r1} - mf_{r2}|. \tag{4}$$

The relationship between n and m for neighboring teeth depends on the number of $f_{r1}/2$ border crossings (j) up to that region, such that $n = m - j$. By comparing these rf frequencies with the recorded ones, we can reconstruct the corresponding optical frequencies. However, to use this technique, we must ensure that the f_{rf} from different regions are unambiguously distinguished. An ambiguity would occur when $k(f_{r1}/2)/\delta f_r$ is an integer, where $k = 1, 2, 3, \ldots$. As shown in Fig. 1(a), channel 4 contains signals from two different regions and hence exhibits ambiguity, while other channels such as channel 2 remain unambiguous. In an experiment, an additional complication may arise due to crosstalk between photodiodes.

To resolve the ambiguity, we rely on the condition:

$$k(f_{r1}/2)/\delta f_r \neq q, \tag{5}$$

where $q = 1, 2, 3, \ldots$. When this condition is satisfied, rf combs originating from different neighboring regions exhibit a relative offset in frequency. This offset can be resolved in the rf domain if the acquisition time is sufficiently long—specifically, longer than the inverse of the relative offset—ensuring that the spectral resolution is finer than the offset itself. The value of the relative offset can be determined by comparing measured signals with simulated rf combs. Depending on the specific configuration of f_{r1} and f_{r2}, not only neighboring spectral regions, but also more distant ones (e.g., neighbors of neighbors, and so on), can exhibit relative offsets. As a result, several distinct spectral regions may be mapped onto distinguishable rf frequencies when captured by a single detector. The maximum number of unambiguous regions that can be simultaneously measured on a single photodetector without ambiguity can be calculated using simulated combs. This constraint is eliminated when a photodiode array is used, as even if identical frequencies appear in nonneighboring spectral regions, they will be captured by different photodiodes, avoiding ambiguity in the recorded data. This effectively limits the achievable unambiguous spectral bandwidth to the emission spectrum of the lasers and the sensitivity range of the photodiodes.

In Fig. 1(b), we present the data acquired with our system. The expected ambiguity in the spectrum as recorded in channel 4 is shown in Fig.1(c). In this case, $\delta f_r \approx$733.04 Hz, so if aliasing were present, there would be only teeth separated by δf_r. However, we observe two sets of comb lines with a relative offset of 283 Hz in the overlapping region of the spectra as shown in the inset (i) of Fig. 1(c). "Unfolding" the data as described above allows us to attribute the spectral peaks to their correct optical frequencies.

One of the major advantages of DCS is its small acquisition time, which is

$$\tau_{\mathrm{min}} = \frac{1}{\delta f_r}, \tag{6}$$

this means fast acquisition rate requires a larger δf_r, however, as shown in Eq. 2, this results in a smaller unambiguity range. Consequently, the same optical bandwidth detected by a photodiode will contain more unambiguous regions. However, with this acquisition speed, it is not possible to eliminate the ambiguity, as the spectral resolution is only sufficient to separate two lines within a single

unambiguous region. For our method, the minimum acquisition time must be at least twice as long to ensure that at least one data point falls between two adjacent lines, enabling the separation of rf combs. Additionally, the repetition rates f_{r1} and f_{r2} must be carefully selected so that the resulting relative offset is resolvable with the available spectral resolution.

Alternatively, one can resolve this ambiguity by aligning the system so that the crossing occurs exactly between two channels. However, when multiple crossings occur across the spectrum, it becomes difficult to tune the system in a way that ensures none of the photodiodes exhibit ambiguity. Instead, addressing these ambiguities during postanalysis using the method described above is significantly easier and more practical.

Experimental setup. The experimental setup (Fig. 2) incorporates a pair of MenloSystems FC1500-250-ULN combs locked to a low phase noise, narrow linewidth (<1 kHz) 1542-nm laser diode (RIO Planex). Then, the repetition rate of each comb follows the laser diode frequency and is stabilized to an FS725 rubidium frequency standard (Stanford Research Systems) via the laser diode. The system generates femtosecond pulses with repetition rates approximately equal to 250 MHz ($f_{r1} \approx 250000240.75$ Hz and $f_{r2} \approx 250000973.79$ Hz) and covers a spectral range from 650 to 2100 nm. The outputs of the two combs are combined using a beam splitter and passed through a samarium (Sm) cell maintained at a temperature of approximately equal to 1040 °C to produce a sufficient density of Sm atoms at a buffer gas (argon) pressure of 330 torr (detailed information about the cell can be found in the Appendix "Samarium Cell Description"). At the temperature and pressure used, the combined Doppler and collisionally broadened linewidth of atomic transitions (on the order of a gigahertz) is sufficiently large, so that several comb teeth (approximately equal to 250-MHz separation defined by the pulse repetition rate) fall under the line profile. The combined light beam is spectrally dispersed with a grating onto the avalanche photodiode (APD) array.

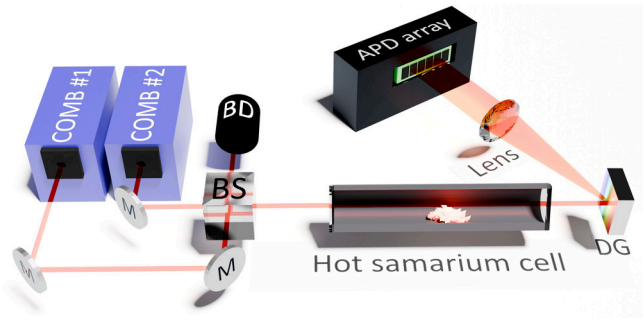

FIG. 2. Schematic of the experimental setup: M, mirror; BS, beam splitter; BD, beam dump; and DG, diffraction grating.

The APD array used in this experiment is Hamamatsu S15249. It consists of 1 × 16 diodes with separate output channels of uniform gain. In this work, only six of them were used as a proof of principle. The array has a spectral response range of 350–1000 nm, with peak sensitivity at 620 nm. We equip each APD channel with a dedicated transimpedance amplifier with a 125-MHz bandwidth, placed as close as possible to the APD array chip, and allowing simultaneous operation across all channels. The common cathode was powered by a linear voltage-stabilized power supply, ensuring low-noise performance, particularly at high frequencies (>50 Hz). The APD of bias voltage was adjusted to optimize the APD gain and achieve the best possible SNR. This choice is motivated by the low output power of the laser in the visible range, where it is critical to ensure that the background noise of the photodetector remains smaller than the laser light noise. In this work, we used the same acquisition system as described for "Apparatus A" in Ref. [12]. Specifically, we used a two-channel digitizer (Spectrum M4i.4420-x8) with a 250-MHz sampling rate and 16-bit resolution. The digitizers' clock frequency was locked to the same rubidium frequency standard as the combs.

The system captures spectra up to 125 MHz (the Nyquist frequency) with a resolution of 0.93 Hz. Data were recorded in chunks of 2^{28} samples per channel (approximately equal to 1.073 s of data) and Fourier transformed on a graphics card in parallel, ensuring continuous acquisition without interruptions. For simplicity, we call it a "one-second" data record. In this work, we did not apply any special window function to the data (a rectangular window was used). The resulting spectra were averaged using the central processor. For details on the data-acquisition system, refer to the Supplemental Material of Ref. [12].

The system imposes no restrictions on the number of spectra that can be averaged. In our experiment, we averaged 1000 spectra per measurement (approximately 17 min). Data from both channels were collected simultaneously. Since the system operates in parallel and each channel functions independently, the number of computers with digitizers can be scaled to enable simultaneous recording across any number of channels. The independent systems can be synchronized using an external trigger.

The high spectral resolution reveals a scalloping pattern between the acquisition system and the rf comb. Various methods can mitigate these artifacts during postanalysis. Our approach involves detecting the peaks of the teeth in the recorded spectrum and redistributing the energy of neighboring bins of the tooth.

Results and discussion. The incident light on each photodiode had an optical bandwidth of approximately 9 nm. As our acquisition system has only two parallel data channels, we performed three sets of two-channel acquisitions (parallel channels: 1&2 | 3&4 | 5&6), covering a total optical range of approximately 52 nm (680 to 732 nm)

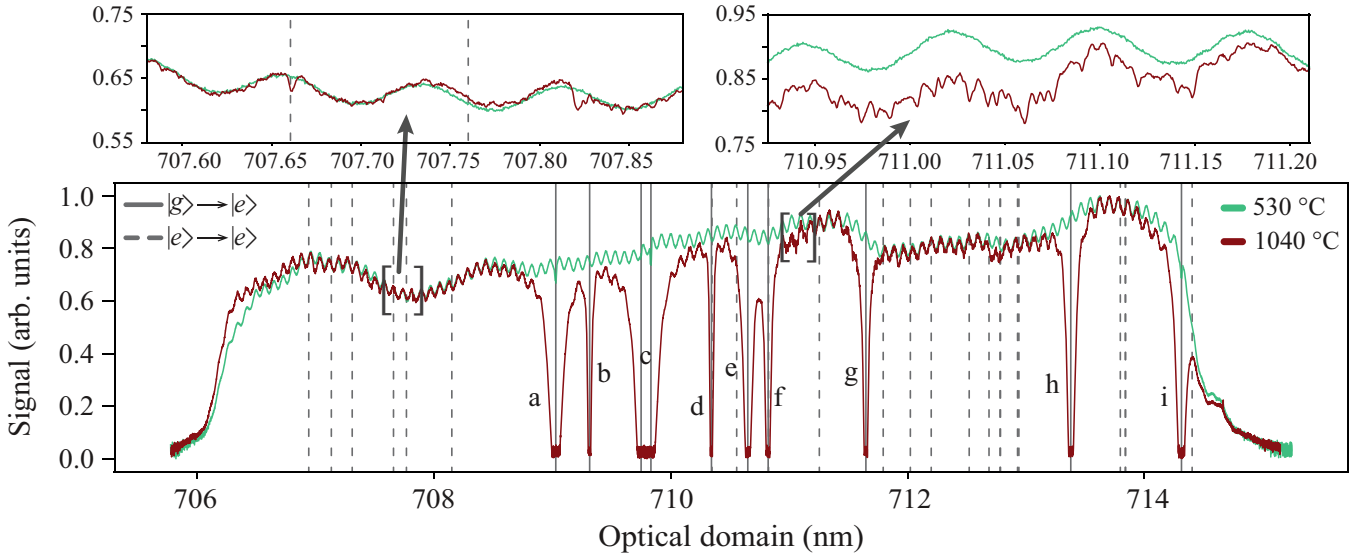

FIG. 3. Absorption spectrum of Sm vapor at various temperatures, obtained by averaging 1000 spectra of one-second records on channel 3, resulting in an SNR of 1100. $|g\rangle$ and $|e\rangle$ represent ground and excited states. The smaller plots show enlarged regions where several unknown lines have been detected. The numerical values of the wavelengths for the detected strong transitions are as follows: a—709.030 nm, b—709.314 nm, c—709.828 nm, d—710.343 nm, e—710.653 nm, f—710.823 nm, g—711.648 nm, h—713.383 nm, and i—714.316 nm.

shown in Fig. 1(b). To maintain a high SNR we averaged 1000 one-second recordings. The SNR varies across the spectrum due to intensity change, as the recorded spectrum lies on the edge of the emission spectrum of the combs. The average SNR is approximately equal to 900, the SNR was calculated as follows:

$$\mathrm{SNR} = \frac{\sqrt{\text{Tooth Height}^2 - \text{Baseline}^2}}{\sigma}, \tag{7}$$

where σ is the standard deviation of the points between two teeth. This approach achieves a DCS figure of merit of $M \times \mathrm{SNR}/\sqrt{\tau} = 3.5 \times 10^6\ \mathrm{Hz}^{1/2}$, and constrained only by the number of the used elements of the photodetector array. In Fig. 3, the most interesting spectrum of the six channels is presented, showing several absorption lines. The high-resolution plots of this spectrum and the remaining channels can be found in the Supplemental Material [13]. We compared measurements taken at different cell temperatures, approximately 530 °C and 1040 °C, to analyze spectral variations at low and high samarium concentrations. These data can also be used to normalize the etalon effect caused by optical elements, which appear as oscillations in the spectrum.

When compared with the existing dataset [14–16], numerous previously unknown lines were detected. Two enlarged subplots illustrate spectral regions with sparse and dense transition lines. To ensure that dense spectral regions are not misinterpreted as system noise, the data at approximately 530 °C is provided, demonstrating that the noise level remains consistent across different spectral regions.

The *d* and *i* transitions, however, were not observed in Refs. [14,16], even though the corresponding energy levels are known. The reason lies in the nature of those experiments: atoms were excited to higher, and even ionized, states and then cascaded down to the ground state. The transitions were detected via fluorescence emitted during this cascade process. Transitions involving the *d* and *i* levels may not have been significantly populated during the cascade and, combined with their lower transition probabilities, likely resulted in the absence of these lines from the recorded spectra [17]. In contrast, in our experiment, atoms are driven directly from the ground state by a resonant field, resulting in strong absorption.

The numerous unidentified transition lines observed in the spectrum arise from the inherent complexity of the Sm atom. In addition to its intricate electronic structure, Sm has five stable isotopes and two long-lived radioactive isotopes with half-lives comparable to, or exceeding, the age of the universe. Some of these lines may also result from two-photon excitations, which can be investigated by analyzing the dependence of the line amplitudes on the laser power.

Conclusion. We present a successful enhancement of the DCS technique by incorporating a photodetector array, effectively addressing the trade-off between SNR and optical bandwidth. It also demonstrates the capability of this technique to acquire a broad spectrum without ambiguity, by introducing a relative offset to rf comb tooth sets from different unambiguity regions. By acquiring data with high spectral resolution, we were able to resolve and reconstruct the unambiguous spectrum. Furthermore, this approach

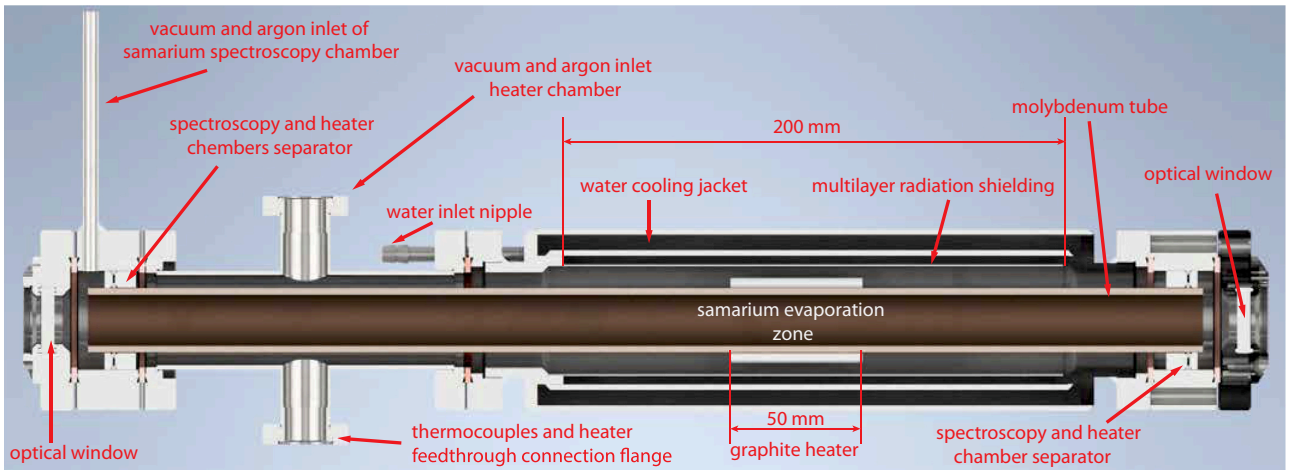

FIG. 4. Schematic of the samarium cell.

enabled the detection of numerous previously unreported transition lines, highlighting its potential for discovering unknown spectral features.

The ability of this system to acquire spectra with both broad bandwidth and high SNR makes it a valuable tool for Spectroscopy 2.0. The next step of this project is to design and implement experiments at high magnetic field environments, up to the 100 T [18,19], to explore the effects of strong fields on atomic transitions.

Acknowledgments. The authors thank Nathalie Picqué, Jason Stalnaker, Arman Cingöz, and Mikhail Kozlov for helpful discussions. This work was supported by the European Commission Horizon Europe Framework Program under the Research and Innovation Action MUQUABIS GA No. 101070546, and by the Deutsche Forschungsgemeinschaft (DFG, German Research Foundation) under Project INST 247/1016-1 FUGG.

Data availability. The data that support the findings of this article are not publicly available upon publication because it is not technically feasible and/or the cost of preparing, depositing, and hosting the data would be prohibitive within the terms of this research project. The data are available from the authors upon reasonable request.

Appendix: Samarium cell description. The spectroscopy cell design Fig. 4 is inspired by the approach of Barkov *et al.* [17], and is engineered to heat solid samarium samples and generate sufficient vapor pressure for absorption and Faraday rotation spectroscopy using continuous-wave lasers, as well as frequency comb spectroscopy.

The cell consists of two separate volumes:

(a) **Inner volume:** This region is dedicated to containing high-purity samarium vapor. It is formed by a molybdenum tube sealed with optical windows and isolated from the outer volume using O-rings compressed between metal sealing rings. Molybdenum is selected for its high melting point, low vapor pressure, and resistance to samarium diffusion into its crystal lattice.

(b) **Outer volume:** The space between the outer surface of the molybdenum tube and a surrounding CF-flanged ANSI 304 stainless steel tube. This region houses thermocouples, electrical wiring, and a graphite heater, which is electrically insulated from the molybdenum tube by an alumina ceramic tube.

The cell design allows the inner and outer volumes to be maintained at different gas pressures. This enables spectroscopic investigation of pressure-dependent features in samarium vapor, while simultaneously allowing the heater to operate in a controlled argon buffer gas environment to reduce degradation and extend operational lifetime.

To minimize radiative heat loss, the inner surface of the stainless steel tube in the hot zone is lined with multilayer heat shields consisting of six layers of polished stainless steel and tantalum foil. The entire assembly is surrounded by a water cooling jacket, which prevents overheating of the stainless steel structure.

Optical windows and fluoropolymer gaskets are positioned as far from the hot zone as possible and maintained at temperatures below 200 °C. Temperatures of both the samarium evaporation zone and the flanges are monitored and controlled using thermocouples.

The maximum temperature achievable in the samarium evaporation zone is approximately 1300 °C, with a total power dissipation of about 1.5 kW.

[1] M. Safronova *et al.*, Search for new physics with atoms and molecules, Rev. Mod. Phys. **90**, 025008 (2018).

[2] A. Kramida *et al.*, (2024). NIST Atomic Spectra Database (version 5.12), [Online]. Available: https://physics.nist.gov/asd. National Institute of Standards and Technology, Gaithersburg, MD. https://doi.org/10.18434/T4W30F.

[3] R. Battesti *et al.*, High magnetic fields for fundamental physics, Phys. Rep. **765766**, 1 (2018).
[4] T. W. Hänsch, Nobel lecture: Passion for precision, Rev. Mod. Phys. **78**, 1297 (2006).
[5] S. Schiller, Spectrometry with frequency combs, Opt. Lett. **27**, 766 (2002).
[6] N. Picqué and T. W. Hänsch, Frequency comb spectroscopy, Nat. Photonics **13**, 146 (2019).
[7] I. Coddington, N. Newbury, and W. Swann, Dual-comb spectroscopy, Optica **3**, 414 (2016).
[8] E. Baumann *et al.*, Spectroscopy of the methane ν_3 band with an accurate midinfrared coherent dual-comb spectrometer, Phys. Rev. A **84**, 062513 (2011).
[9] Z. Wei *et al.*, The development and application of dual-comb spectroscopy in analytical chemistry, Chin. Chem. Lett. **34**, 107254 (2023).
[10] N. R. Newbury *et al.*, Sensitivity of coherent dual-comb spectroscopy, Opt. Express **18**, 7929 (2010).
[11] Y. Sugiyama *et al.*, Precision dual-comb spectroscopy using wavelength-converted frequency combs with low repetition rates, Sci. Rep. **13**, 2549 (2023).
[12] O. Tretiak *et al.*, Improved bounds on ultralight scalar dark matter in the radio-frequency range, Phys. Rev. Lett. **129**, 031301 (2022).
[13] See Supplemental Material at http://link.aps.org/supplemental/10.1103/7ktx-4h8m for high-resolution plots of the spectrum.
[14] C. Ferrara *et al.*, Experimental atomic data of spectral lines - I. Cs, Ba, Pr, Nd, Sm, Eu, Gd, Tb, Dy, Ho, Er, Tm, Yb, Lu, Hf, Re, and Os in the 370–1000 nm interval, Mon. Not. R. Astron. Soc. **527**, 4440 (2023).
[15] W. Martin *et al.*, Atomic Energy Levels - The Rare-Earth Elements: The Spectra of Lanthanum, Cerium, Praseodymium, Neodymium, Promethium, Samarium, Europium, Gadolinium, Terbium, Dysprosium, Holmium, Erbium, Thulium, Ytterbium, and Lutetium, Nat. Stand. Ref. Data Ser., Nat. Bur. Stand. (U.S.) **60**, 422 (1978).
[16] W. F. Meggers *et al.*, Tables of Spectral-Line Intensities: Part 1- Arranged by Elements, Nat. Bur. Stand. (U.S.), Monogr. **145**, 403 (1975).
[17] L. Barkov *et al.*, Study of the $4f^6 6s^2\, ^7F \rightarrow 4f^6 6s^2\, ^5D$ forbidden transitions of atomic samarium, Opt. Spectrosc. (USSR) **66**, 288 (1989).
[18] B. Hervieu *et al.*, Cryogenic design of the 43 T LNCMI Grenoble hybrid magnet, Phys. Procedia **67**, 692 (2015).
[19] J. Beard *et al.*, Design and tests of the 100-T triple coil at LNCMI, IEEE Trans. Appl. Supercond. **28**, 1 (2018).